J. Earth Syst. Sci. (2020)129 9
https://doi.org/10.1007/s12040-019-1272-9

Dimensionality analysis of MT data using Mohr circle: A case study from Rewa–Shahdol region, India

Khasi Raju and Prasanta K. Patro*

Magnetotelluric Division, CSIR–National Geophysical Research Institute, Hyderabad 500 007, India.
**Corresponding author. e-mail: patrobpk@ngri.res.in*

MS received 14 February 2019; revised 23 July 2019; accepted 26 July 2019

Mohr circle in magnetotelluric (MT) is being used to represent dimensionality of subsurface structure. Mohr circle plot on individual axes for each frequency represents the dimensionality concerning frequency, whereas plotting of Mohr circle on common Cartesian coordinates for all frequencies displays the effects of noise on the impedance tensor. Here, we examine the Rewa–Shahdol region MT data with the Mohr circle approach to understand the sub-surface dimensionality structure, but the presence of noise in the signal has randomized the Mohr circle response. Hence, we made an effort to obtain the subsurface dimensionality using Mohr circle properties and derive two new invariants such as $\tan\phi$ and $\sin\theta$. The two invariants represent the dimensionality and anisotropy nature of the subsurface structure. Results from the Mohr circle together with the new angles brought out the 1-D graben structure of the Gondwana and Vindhyan basins, 2-D/3-D nature of the underlying basement structure and the crustal structure below the Narmada–Son Lineament (NSL) zone. 2-D/3-D nature of the NSL zone represents the basement uplifted horst structure between Gondwana and Vindhyan basins. Further, the horst-graben structure of NSL zone is evident from the Mohr circle analysis suggesting of rifting and block movement.

Keywords. Mohr circle; Rewa–Shahdol region; magnetotelluric; Narmada–Son lineament.

1. Introduction

Otto Mohr introduced Mohr's Circle in 1882, to represent transformation equation for plane stress in graphical form. Lilley (1976) adopted the Mohr circle to represent magnetotelluric (MT) impedance tensor information in terms of one and two-dimensionality structures. Later on, Lilley (1993a) considered real and imaginary parts separately to plot Mohr circle and extended the Mohr circle applications to represent three-dimensional structure, anisotropy angle, skew angle, and Groom-Bailey decomposition technique. Lilley (1993a) brought out several invariants, which can be represented by the Mohr circle. Lilley (1993b) shows a particular pattern of Mohr circle that indicates the effect of local static shift over a 1-D structure. He also described the Bahr skew angle in connection with the Mohr circle to identify certain classes of local distortion in MT data. In this study, we attempt to extract the dimensionality of the subsurface structure along the MT profile in Rewa–Shahdol region using Mohr circle and its properties such as radius of Mohr circle and the center point of Mohr circle, central impedance and first effective impedance. Also, we proposed two new invariant parameters, i.e., $\tan\phi$ and $\sin\theta$, which are derived from Mohr circle radius, first effective impedance, mean of diagonal elements and central impedance to study the dimensionality and structure below the Rewa–Shahdol region. Before examining the real data, we analyze

Published online: 19 December 2019

synthetic random noise added good quality MT data with two types of plots such as plotting Mohr circle on individual axes for each frequency (Type-I) and Mohr circle on common axes for all frequencies (Type-II) to understand the variation of Mohr circle and its properties with noisy data and noise-free data.

2. Generation of Mohr circle

To plot the Mohr circle, $Z'xy_r, Z'xx_r$ (subscript r indicates the real components of impedance tensor) are used as abscissa and an ordinate respectively, these are generated by clockwise rotation of measured tensor, i.e., Zxy_r and Zxx_r.

Real and imaginary parts of observed tensor

$$\begin{bmatrix} Zxx_r & Zxy_r \\ Zyx_r & Zyy_r \end{bmatrix} \text{ and } \begin{bmatrix} Zxx_i & Zxy_i \\ Zyx_i & Zyy_i \end{bmatrix}. \quad (1)$$

The measured tensor (Z) is rotated to principal axes for two-dimensional impedance tensor analysis of magnetotelluric data.

The rotation operator is

$$R(\alpha) = \begin{bmatrix} \cos\alpha & \sin\alpha \\ -\sin\alpha & \cos\alpha \end{bmatrix} \text{ and}$$

The rotation angle is given by

$$Z(\alpha) = R(\alpha)ZR(-\alpha)$$

(Simpson and Bahr 2005).

$$\text{Rotated real part of the tensor} \begin{bmatrix} Z'xx_r & Z'xy_r \\ Z'yx_r & Z'yy_r \end{bmatrix}, \quad (2)$$

$$\text{Rotated imaginary part of the tensor} \begin{bmatrix} Z'xx_i & Z'xy_i \\ Z'yx_i & Z'yy_i \end{bmatrix}. \quad (3)$$

Mohr circle is generated on $Z'xy_r, Z'xx_r$ axes using circle center points (C1, and C2) and radius (R).

$$\text{C1} = \frac{1}{2}(Zxy_r - Zyx_r), \quad (4a)$$

and

$$\text{C2} = \frac{1}{2}(Zxx_r + Zyy_r) \text{ (real part only)}, \quad (4b)$$

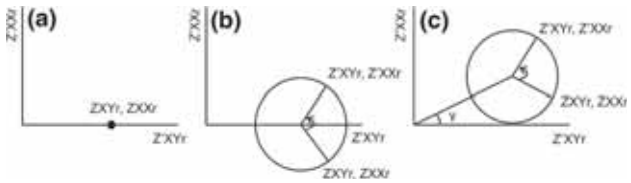

Figure 1. Graphical representation of the Mohr circle for 1-D (**a**), 2-D (**b**) and 3-D (**c**) responses of MT impedance tensor (real component only). Clockwise rotation (with θ) values ($Z'xy_r, Z'xx_r$) of measured tensor (Zxy_r, Zxx_r) plotted against each other (i.e., $Z'xy_r$ abscissa, $Z'xx_r$ ordinate). Anticlockwise rotation (2θ) of a measured tensor is represented by $Z'xy_r, Z'xx_r$. Skew angle (γ) indicates the deviation of the circle from horizontal axes (**c**) (modified after Lilley 1993a).

the radius of the circle (R)

$$= \frac{1}{2}\left[(Zxx_r - Zyy_r)^2 + (Zxy_r + Zyx_r)^2\right]^{1/2} \quad (5)$$

(real part only).

For 1-D structure, measured tensor shows $Zxx = Zyy = 0$ and $Zxy = -Zyx$, a consequence of these, Mohr circle radius (equation 5) and the center points (equation 4a and b) ultimately represent 1-D structure as circle radius reduce to the center point of the circle (figure 1a) on the horizontal axis. In case of 2-D ($Zxx = -Zyy$ and $Zxy \neq -Zyx$) the radius (equation 5) and the center point of the Mohr circle (equation 4a and b) represent 2-D responses as the center point of the circle lie on or very near to horizontal axis (figure 1b). 3-D responses obtained when the circle moves away from the horizontal axis (figure 1c), and the deviation of the circle from the horizontal axis represents the skew angle (γ). The orientation of radial arm in the Mohr circle indicates the direction of geological strike, which can be drawn from the center point of the circle to the measured point of tensor on the circumference of the circle (Lilley 1993a). If the radial arm direction is parallel in real and imaginary parts of the circle, then it

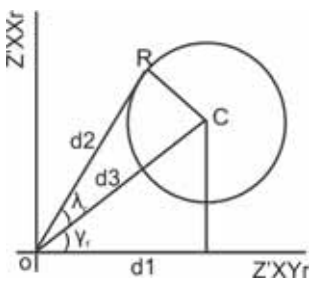

Figure 2. Real parts of first effective impedance (d2), second effective impedance (d1), central impedance (d3), anisotropy angle (λ) and skew angle (γ) are plotted (modified after Lilley 1993a).

indicates the 2-D subsurface and non-parallel of the radial arm in real and imaginary parts indicates 3-D structure (Bayrak *et al.* 2000 and references therein).

Lilley (1993a) proposed following invariants, which are related to the Mohr circle properties (see figure 2). These are, first effective impedance (d2), second effective impedance (d1) and central impedance (d3).

First effective impedance (d2)

$$= (ZxxZyy - ZxyZyx)^{1/2},$$

Second effective impedance (d1)

$$= \frac{1}{2}(Zxy_r - Zyx_r),$$

Central impedance (d3)

$$= \frac{1}{2}\left[(Zxx_r + Zyy_r)^2 + (Zxy_r - Zyx_r)^2\right]^{1/2}.$$

The standard errors (given below) for coordinates of Mohr circle and Mohr circle radius are proposed by Lilley (1993c) to measure the accuracy of Mohr circle coordinates and radius. These errors were propagated to the plotting of Mohr circle properties.

The standard error in the abscissa of the circle center is

$$\mathrm{e1} = \frac{1}{2}(\mathrm{e}Zxy_r + \mathrm{e}Zyx_r).$$

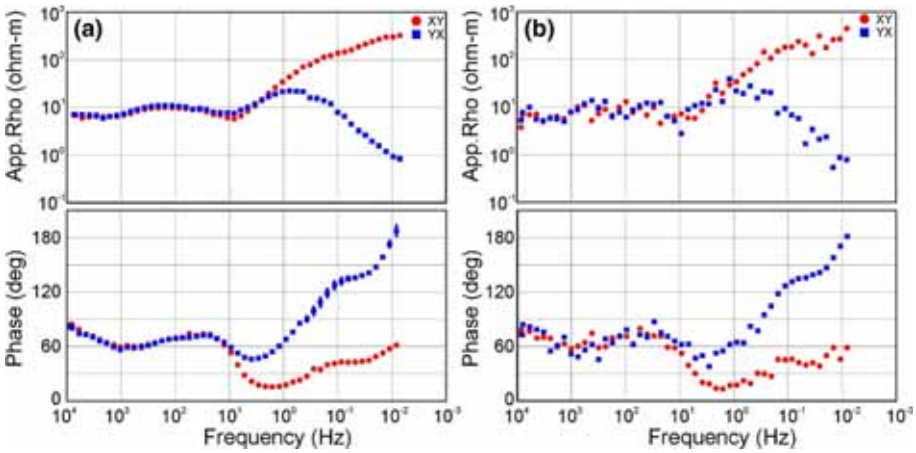

Figure 3. Resistivity and phase curves of RO station before adding synthetic noise (**a**) and after adding of synthetic noise (**b**).

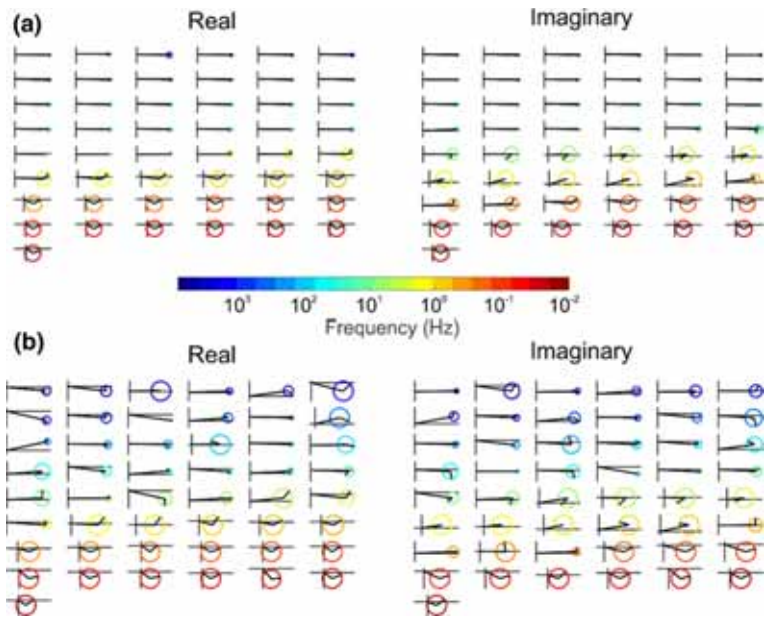

Figure 4. Representation of Mohr circle response (real and imaginary parts) on individual axes for each frequency of RO station before (**a**) and after (**b**) adding the synthetic random noise.

The standard error in the ordinate of the circle center is

$$\mathrm{e2} = \frac{1}{2}(\mathrm{e}Zxx_r + \mathrm{e}Zyy_r),$$

and the error in circle radius estimated as

$$\mathrm{e3} = \frac{1}{2}\mathrm{e4}/R,$$

here

$$\mathrm{e4} = \mathrm{e1}(|Zxy_r + Zyx_r|) + \mathrm{e2}(|Zxx_r - Zyy_r|),$$

and R is the radius of the Mohr circle.

The arithmetic mean of diagonal elements (D) can be written as $\frac{1}{2}(Zxx_r + Zyy_r)$. In the preceding section, the arithmetic mean of diagonal impedances (D) and the radius of the circle responses are plotted together to interpret the randomized Mohr circle response. In the Mohr circle plot, D controls the vertical movement of the circle along the horizontal axis; this movement notifies the dimensionality of the subsurface structure. When the value of D becomes zero, it indicates the 1-D or 2-D subsurface structure and non-zero D values indicate the three-dimensionality of the structure. Similarly, the Mohr circle radius (R) also becomes zero for 1-D and non-zero for 2-D and 3-D. In the Mohr circle properties plot, analyzing both D and R together brings out the dimensionality of the subsurface with much clarity.

3. A synthetic study using real MT data added with random noise

To understand the role of noise on the Mohr circle response, we have conducted a synthetic study, in which, we have added synthetic random noise (10% of signal) to an MT site RO, having good quality data, to ensure substantial variation in the Mohr circle responses with noise and without noise. The addition of noise did not bring changes in the MT data trend whereas; one can observe a clear variation in the Mohr circle plots before and after adding the noise. The procedure of adding random noise to the real data is discussed below:

Percentage of noise in the signal (x)
$= 0.1 * Zxy$ or Zyx,

Variation in amplitude$(v) = 1.5$,

Noisy signal $(y) = x *$ random noise $+ v$.

Impedance elements after adding the noise are

$$Zxx1 = Zxx + y,$$

$$Zxy1 = Zxy + y,$$

$$Zyy1 = Zyy + y,$$

$$Zyx1 = Zyx + y.$$

We present real data before adding synthetic random noise and after adding synthetic random noise in figure 3(a and b), respectively. It may be seen from figure 3(b) that the addition of noise to

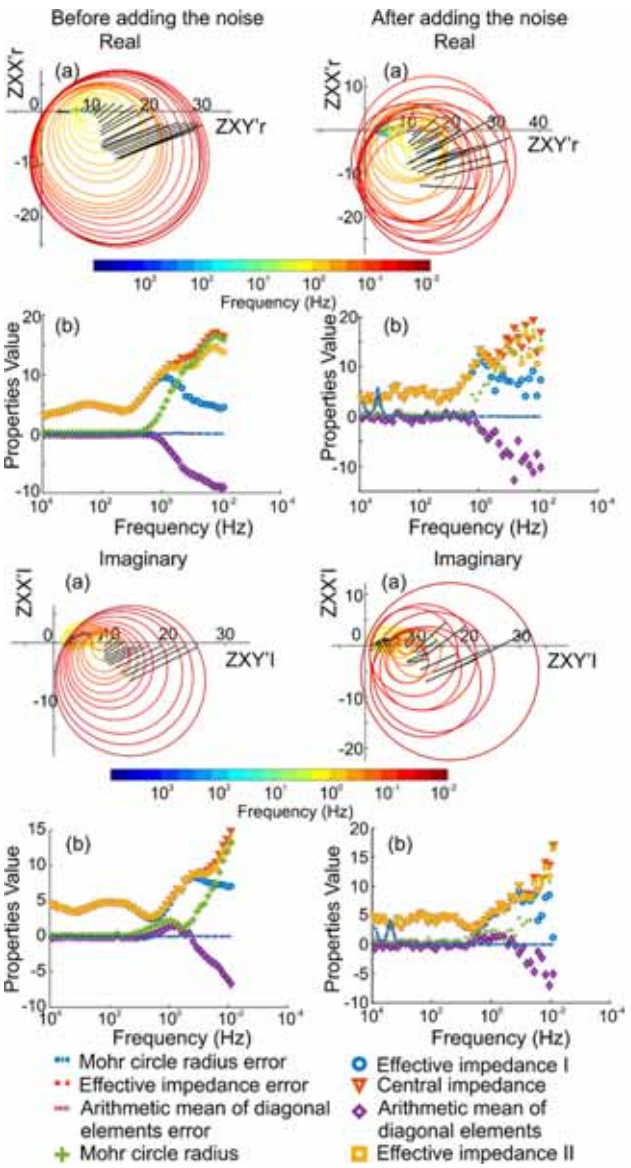

Figure 5. The response of the Mohr circle and its properties before adding the noise (left side) and after adding the noise (right side). The top figure is a real part response, and imaginary part results show the bottom figure.

the good quality MT data brought out scatter in the resistivity and phase data.

3.1 *Mohr circle on individual axes (Type-I plot)*

We plot Mohr circle on individual axes for each frequency components at MT site 'RO' before and after adding the synthetic random noise (see figure 4a and b). Plotting of Mohr circle on individual axes for each frequency describes the variation of dimensionality with respect to the frequency. This plot also shows the influence of an unwanted signal on the Mohr circle response at each frequency component. The Mohr circle response of RO station before and after adding the noise is shown in figure 4, in which 1-D structure appears at the high-frequency (figure 4a) in real and imaginary parts before adding the noise, but after adding the noise, Mohr circle behaves in a random manner (figure 4b). We can observe a significant variation between Mohr circle plots before adding the noise and after adding the noise at the high-frequency range. Whereas, at lower frequency range, we do not notice a considerable difference between the two responses (figure 4a and b).

3.2 *Mohr circle on common axes (Type-II plot)*

In the type-II plot, abscissa and ordinate were considered as common to represent Mohr circle for all frequencies of impedance tensor. We plot the Mohr circle for RO station data set before and after adding the synthetic random noise (figure 5). Mohr circle (real and imaginary parts) shows a symmetrical nature before adding the noise (left-side part of figure 5a). However, it becomes asymmetric after adding random noise to the data (see the right-side part of figure 5a). In the type-II plot, the presence of noise in the signal is represented by a solid deviation between the Mohr

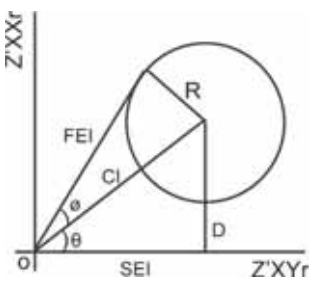

Figure 6. The image is showing the Mohr circle and its properties. The $\tan\phi$ derived from the ratio of the radius (R) and first effective impedance (FEI). The ratio of Mohr circle y-coordinate (D) and central impedance (CI) produced $\sin\theta$.

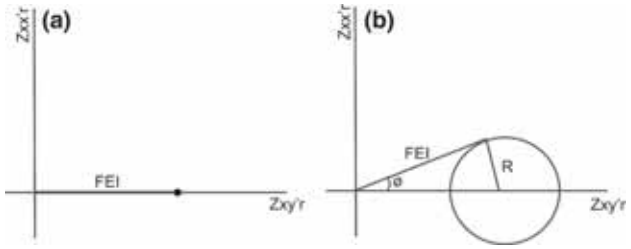

Figure 7. Representation of dimensionality using Mohr circle radius and first effective impedance. Angle zero indicates the 1-D structure (**a**) and non-zero angle obtained when the structure is 2-D or 3-D (**b**).

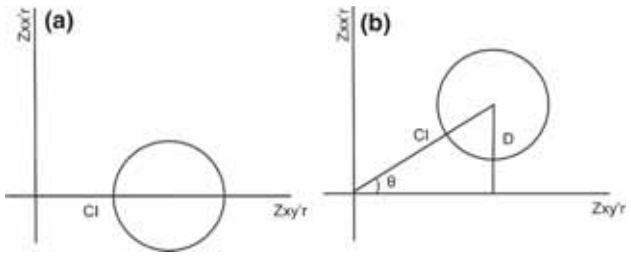

Figure 8. Representation of dimensionality using Mohr circle center point (y-coordinate or D) and central impedance. The angle zero indicates the 1-D or 2-D structure (**a**) and non-zero angle obtained when the structure is 3-D (**b**).

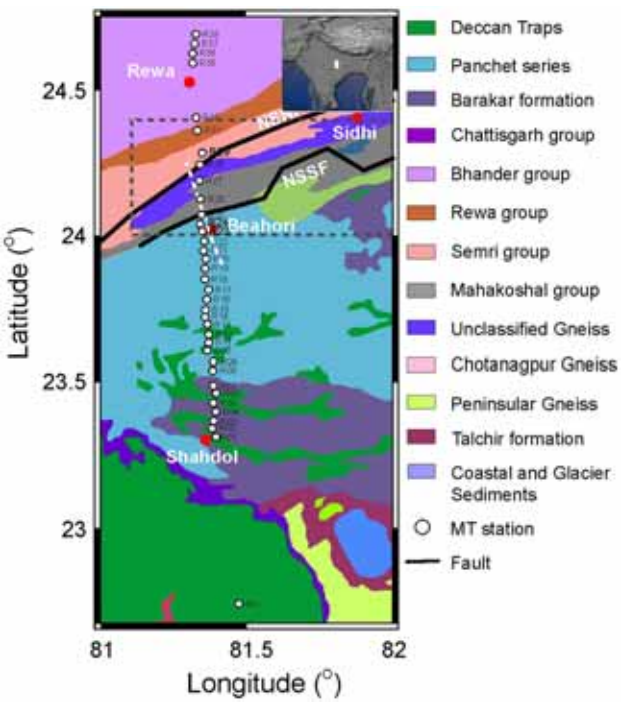

Figure 9. Geological formations and MT station locations of Rewa–Shahdol region of Madhya Pradesh state, India. The image also shows the accomplished gravity studies by CRUMANSONATA (1995) (dashed white line) and Qureshy and Warsi (1975) (grey color dashed rectangular box) also, representing Narmada–Son South Fault (NSSF) and Narmada–Son North Fault (NSNF) in this region (modified after Geological and Mineral map of Madhya Pradesh and Chhattisgarh, Geological Survey of India, 2005).

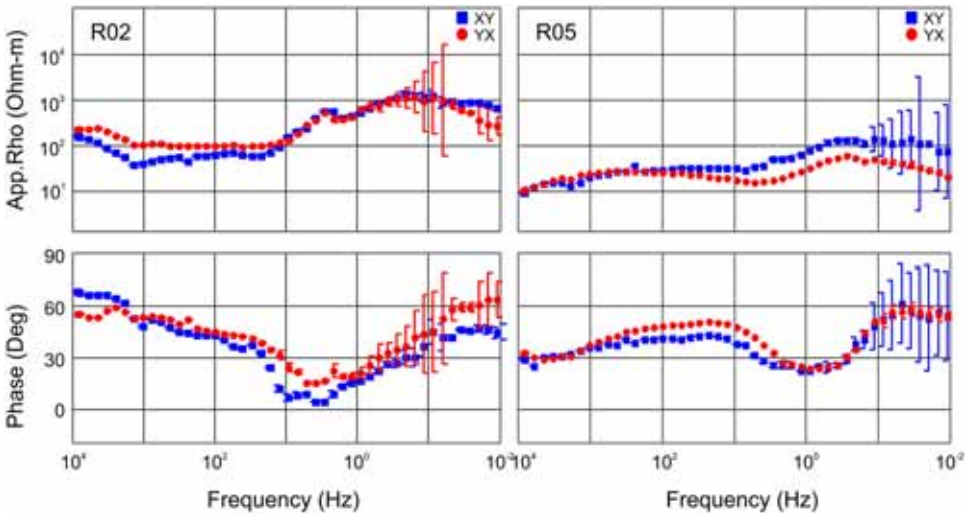

Figure 10. Apparent resistivity and phase responses of R2 and R5 stations, which are measured in geographic coordinates (X, North–South; Y, East–West).

circle responses before adding the noise and after adding the noise. The direction of the radial arm in real and imaginary part should be parallel for 2-D structure, and the direction depart from parallel for 3-D structures (Bayrak *et al.* 2000 and references therein). Whereas in our study, we do not observe such a scenario as the radial arm direction being parallel in real and imaginary parts, but Mohr circle properties show 3-D signature at the lower-frequency as shown in figure 5(a). Properties of Mohr circle such as radius, center points, and central impedance plotted together with respect to the frequency before and after adding the noise (figure 5b). Before adding the noise, all the properties show smooth variation along the frequency whereas, after addition of noise to the data, the Mohr circle properties scatter along the frequency.

4. New invariants ($\tan\phi$ and $\sin\theta$)

So far, we have discussed the plotting of the Mohr circle with two different types. Here, we propose two angles such as $\tan\phi$ and $\sin\theta$ to envisage dimensionality of subsurface structure, and that can be represented on the Mohr circle, as shown in figure 6. The $\tan\phi$ is obtained from the Mohr circle radius and the first effective impedance.

$$\tan\phi = \frac{\text{Radius of Mohr circle } (R)}{\text{First effective impedance (FEI)}},$$

and the $\sin\theta$ is formed from the mean of diagonal element and central impedance (figure 6).

$$\sin\theta = \frac{\text{Mean of diagonal elements } (D)}{\text{Central impedance } (CI)}.$$

These angles also represent distortion conditions and anisotropy state in the MT data.

4.1 *Properties of $\tan\phi$ and $\sin\theta$: Identification of 1-D and 2-D*

As discussed in section 2, for a 1-D Earth, wherein conductivity varies only with depth, the diagonal elements of the impedance tensor, *Zxx* and *Zyy* are zero, while the off-diagonal (*Zxy* and *Zyx*) components are equal in magnitude, but have opposite signs. Hence, the Mohr circle radius (equation 5) will be zero for 1-D structure, a consequence of that, $\tan\phi$ eventually represents the 1-D structure when the angle becomes zero (figure 7a). For a 2-D Earth, conductivity varies along one horizontal direction as well as with depth, in which *Zxx* and *Zyy* are equal in magnitude, but have opposite sign, whereas *Zxy* and *Zyx* differ. In that case, the Mohr circle radius will be non-zero, then the $\tan\phi$ shows above zero values (figure 7b) that may represent the 2-D or 3-D structure.

4.2 *Identification of the 3-D structure*

Non zero values of $\tan\phi$ represent the 2-D or 3-D structure; thus, to distinguish the 2-D and 3-D structure, we proposed a new invariant '$\sin\theta$' using the mean of diagonal elements and central impedance. For 2-D structure, *Zxx* and *Zyy* are equal magnitude but have opposite sign. Here, the mean of diagonal elements will be zero; then, the $\sin\theta$

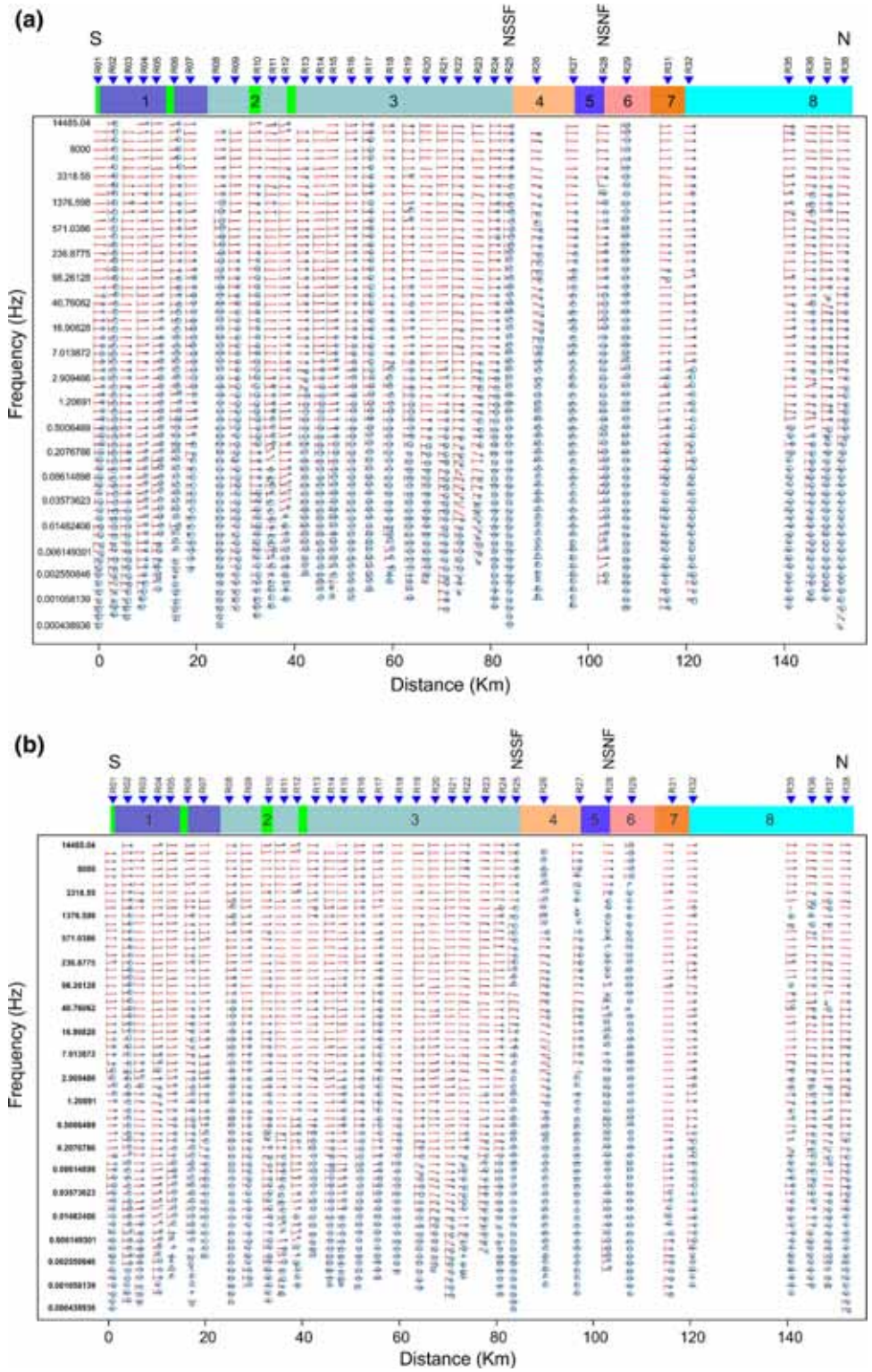

Figure 11. (**a**) Mohr circle representation (real part) on individual axes for each frequency of entire profile length. Also, present surface geological formations along the profile. (**b**) Mohr circle representation (imaginary part) on individual axes for each frequency of entire profile length. Also, present surface geological formations along the profile. (1) Barakar formation; (2) Deccan traps; (3) Bhander group; (4) Mahakoshal group; (5) Unclassified Gneiss; (6) Semri group; (7) Rewa group; (8) Bhander formation.

becomes zero, as shown in figure 8(a). For a 3-D structure, all impedance elements will become non-zero. Thus, $\sin\theta$ bring out the 3-D signature when the angle becomes >0 (figure 8b). The angle near or above 90° indicates the distortion or anisotropy in the MT data set.

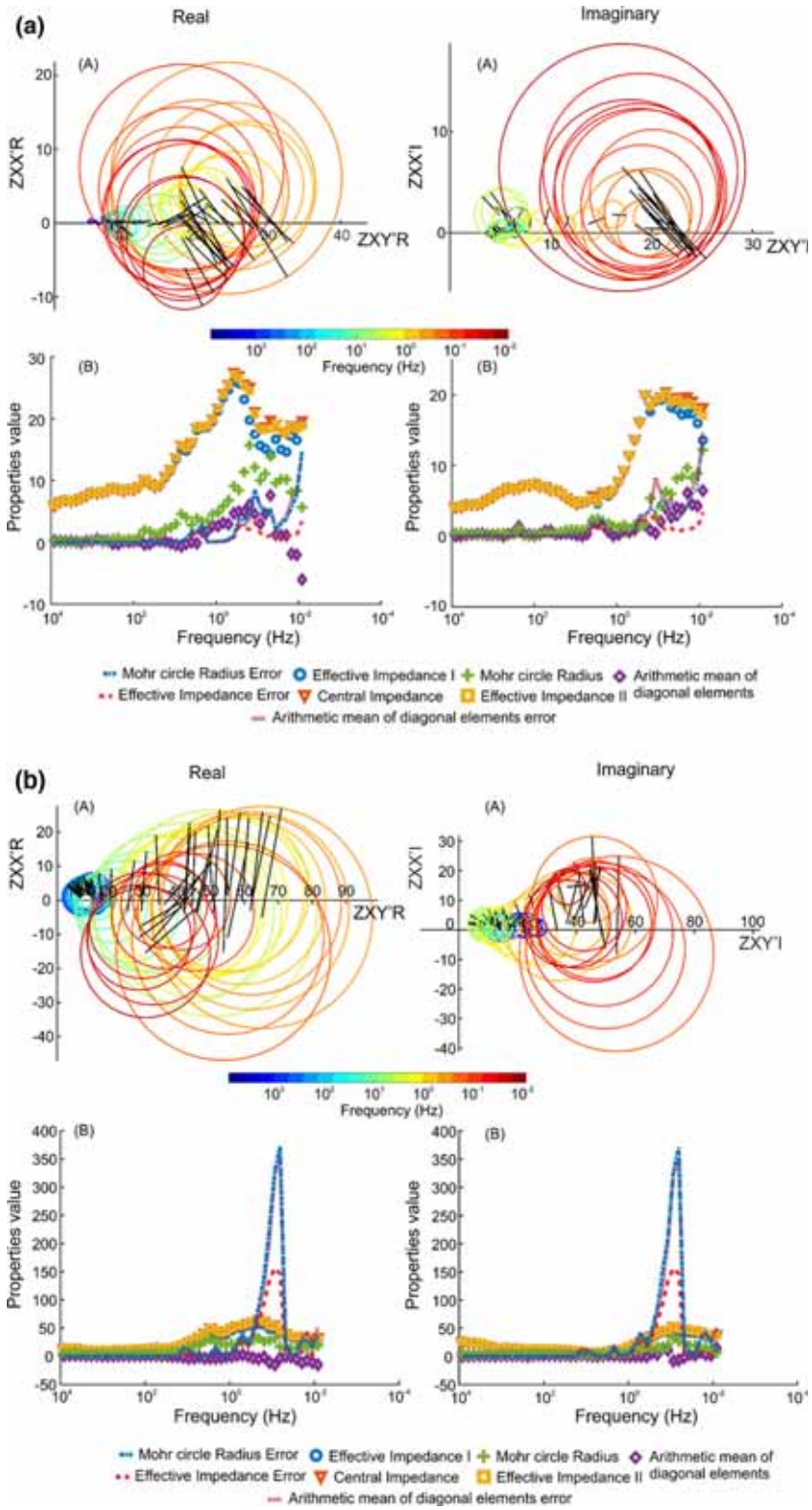

Figure 12. Real and imaginary parts of Mohr circle on common axis (figure A) and Mohr circle properties plot with respect to the frequency (figure B) for R1, R2, R3, R4 and R5 MT stations in figure 12(a–e), respectively. In figure 12d (B), the arithmetic mean of diagonal elements and Mohr circle radius values fluctuated at the 1-D condition (rectangular box).

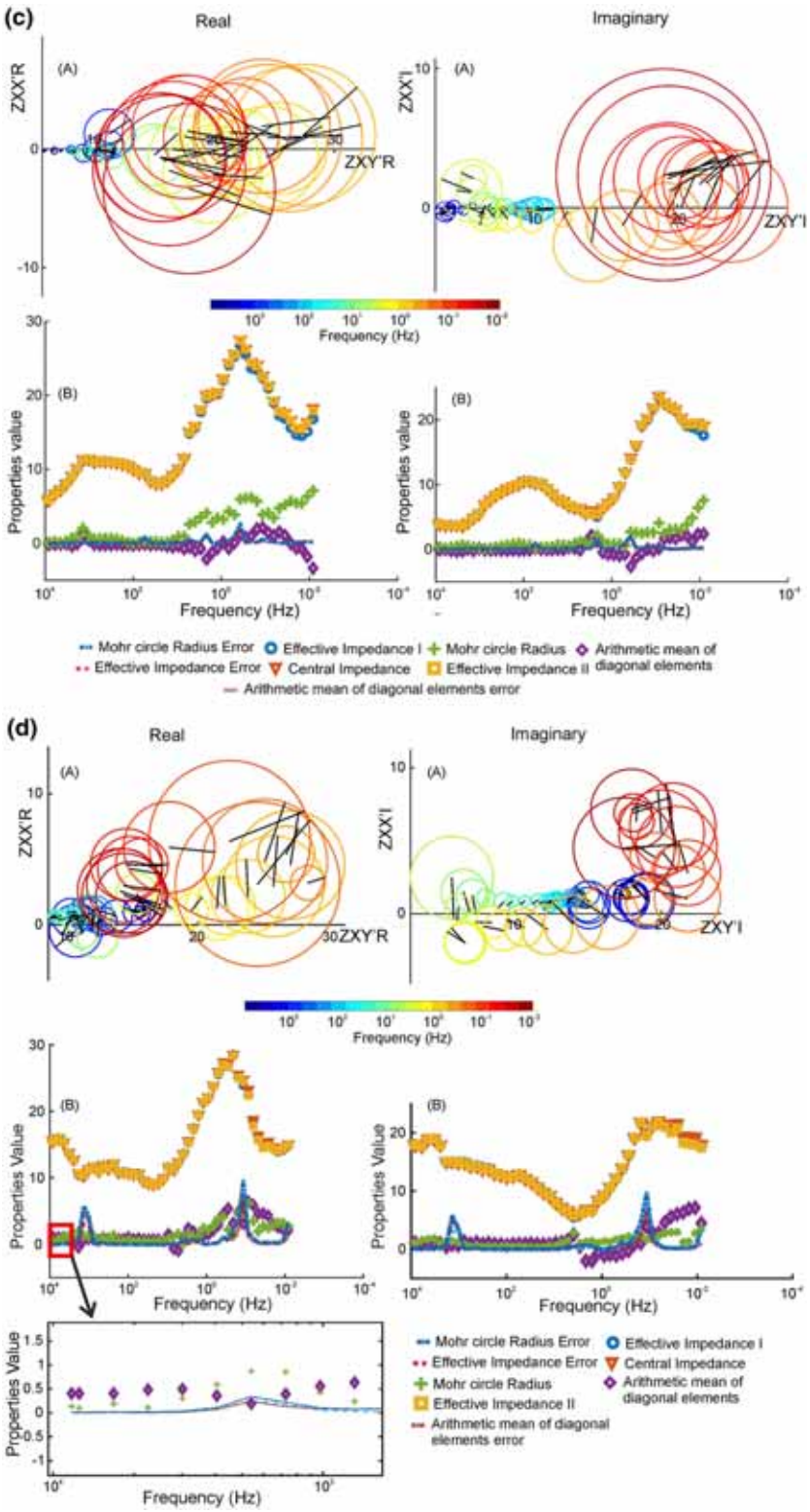

Figure 12. (*Continued.*)

5. Application to Rewa–Shahdol region, India

Rewa–Shahdol region is situated in the eastern segment of Central India Tectonic Zone (CITZ), and the region is covered with different geological formations such as Deccan trap, Upper Gondwana, Lower Gondwana, Vindhyan group and Mahakoshal group (figure 9). CITZ is a prominent tectonic zone in the Indian subcontinent after Himalayas seismotectonic zone. It was formed by accretion of southern craton of India (Bastar) and

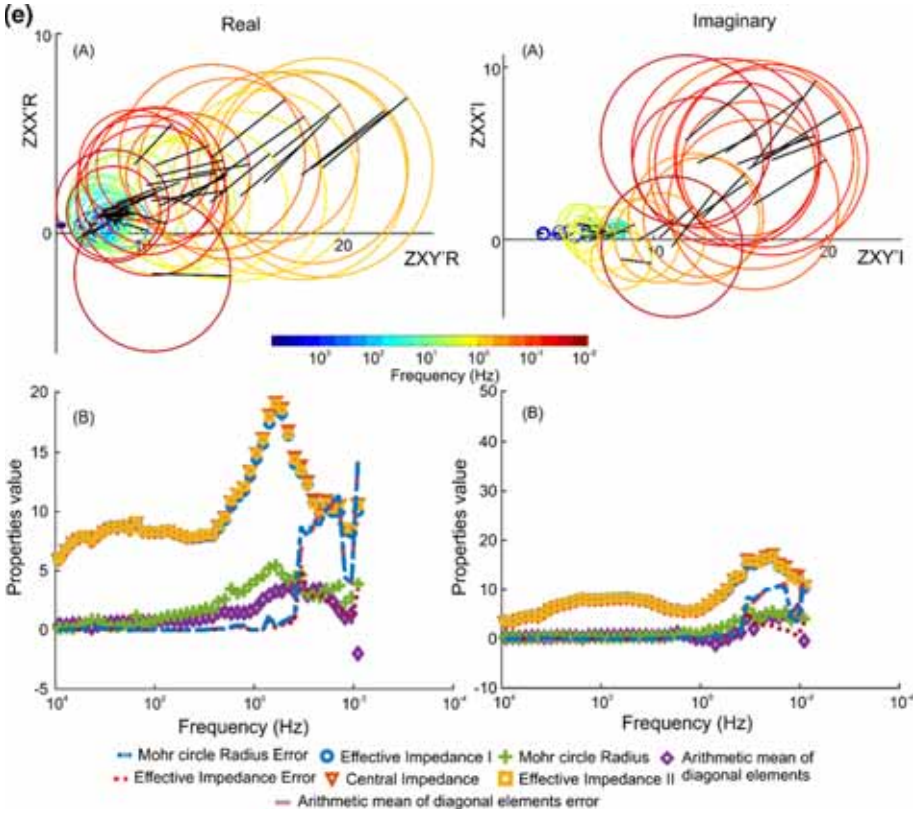

Figure 12. (*Continued.*)

northern craton of India (Bundelkhand craton) during Paleo to the Neoproterozoic period (Roy and Prasad 2001). CITZ leads the main role to accumulate several Gondwana sedimentary basins along the lineament, which are bounded by faults and shear zones (Chakraborty *et al.* 2003). Narmada–Son lineament (NSL) is a salient geological feature in the northern boundary of CITZ, and it controlled the Gondwana and the Vindhyan sedimentary formations to spread across the NSL (West 1962; Choubey 1971). The NSL was uplifted, warped, rift faulted and accompanied by the development of tensional faults which are generally dyke-filled extension fractures through which the extrusion of a great number of tholeiitic basalts and smaller quantities of more basic and more acidic types occurred (Choubey 1971). During the crustal resetting process, high-density Mahakoshal group (MG) rocks replaced the low-density continental crust in the NSL zone. The MG rocks are bounded by two prominent faults, i.e., Narmada–Son South Fault (NSSF) and Narmada–Son North Fault (NSNF) (Rao *et al.* 1990). Repeated reactivation of MG brought out several phases of concordant, sheet-like granitic plutons that were emplaced all along the fault zone (Roy and Prasad 2003). Roy and Bandyopadhyay (1990) suggested that the MG belt represents an aborted crustal rift structure in Bundelkhand region. Deep seismic studies by Kaila *et al.* (1987) suggested that NSL represents a basement uplifted fault zone in the form of a horst structure that played a main role during the sedimentation on either side of the NSL. Murty *et al.* (1998) revisited the seismic study of Kaila *et al.* (1987) and proposed that the NSL zone is represented by upwarp in the Moho boundary. MT studies (Rao *et al.* 1995, 2004; Gokarn *et al.* 2001; Patro *et al.* 2005; Naidu and Harinarayana 2009; Azeez *et al.* 2013) were conducted in central and western part of the NSL zone to understand the tectonic setting and delineate the geological structures. Most of the MT studies brought out discrete conductivity bodies (10–100 ohm-m) in the depth range of 3–30 km. Patro and Sarma (2016) suggested that emplacement of mafic material during the Deccan volcanic episode responsible for the high conductivity in the NSL zone.

Several studies were conducted in the western and central part of the NSL, whereas, in the eastern segment of the NSL, not many geophysical studies have been carried out. Also, the evolution

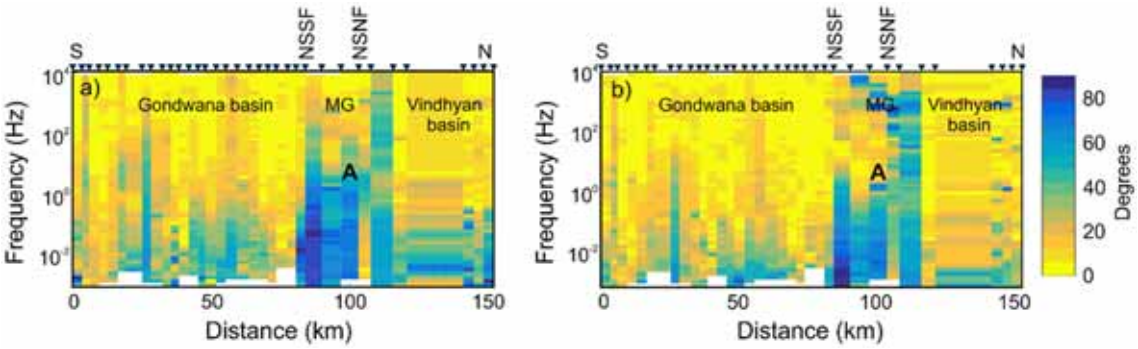

Figure 13. Pseudosection of tan ϕ (real and imaginary components) derived from the MT data from Rewa–Shahdol region. Color scale indicates the range of angle. The real component is plotted in the left (**a**) and the imaginary component is plotted to the right (**b**). The image shows high values of tan ϕ ('A' in this figure) below the NSL region comprising of NSSF and NSNF. MG: Mahakoshal Group of rocks.

of the CITZ, including the origin of Gondwana basins is still under debate. To understand the deep crustal structure and the deposition environment of Vindhyan and Gondwana basins in central India, we have adopted the magnetotelluric technique in Rewa–Shahdol region, India.

6. MT data

Magnetotelluric data were collected along 150 km long profile at 38 stations using a broadband MT data logger (M/s Metronix, Germany). The orientation of measured data x-axis and y-axis are situated along north–south and east–west directions, respectively. We maintained one remote station for an entire period of the field campaign to achieve more reliable results when the base station data is noisy. MT data were processed using MAPROS (M/s Metronix, Germany) software package. This package provides single-site estimates of transfer function using different processing methods such as selective stacking, coherency threshold, stack all, and remote reference. Most of the stations in the northern part of the profile are contaminated with noise. Hence, remote reference processing was adopted to improve the data quality. Few typical MT data (apparent resistivity and phase) are presented in figure 10. At the MT stations R2 and R5, the low frequency contains mostly error bars that might be due to the cultural noise. We made an effort to improve the data at a lower frequency by using remote reference technique and at higher frequency range, the data were improved applying notch filter. Further, we have adopted a systematic approach for data processing, as suggested by Borah *et al.* (2015) and improved the transfer functions for an entire frequency range.

6.1 *Type-I plot*

We examine the MT data from Rewa–Shahdol region with the Mohr circle to empathize the dimensionality of the subsurface structure along the profile. The Mohr circle plot for Rewa–Shahdol region MT data with respect to the frequency demonstrates the variation of dimensionality at each frequency component, as shown in figure 11a and b. As discussed in the synthetic study, Mohr circle response for the high-frequency range is most vulnerable to noise than the low-frequency range response. Mohr circle plot for Rewa–Shahdol region MT data also shows an irregular response due to the noise over the high-frequency range at some stations whereas, at lower frequency range, Mohr circle showing consistency response.

Anomalous behavior of the Mohr circle below the NSL for an entire frequency range suggests the 2-D/3-D subsurface signature (figure 11a and b). Also, for the low-frequency range, the Mohr circle crosses the vertical axis in real and imaginary parts. Lilley (1993b) proposed that, when Mohr circle crosses the vertical axis, it shows the high anisotropy or 2-D distortion. In Type-I plot, R02, R06, R08, and R17 stations showing 2-D signature at the high-frequency in the real part of Mohr circle whereas the 2-D feature is unclear in the imaginary part. Except for R02, R06, R08, R17, R25, R26, R27, R28, and R29 rest of stations are showing 1-D signature up to 96 Hz in both components. At lower frequency range, the Mohr circle plots at all MT stations show a 2-D/3-D signature in the study area.

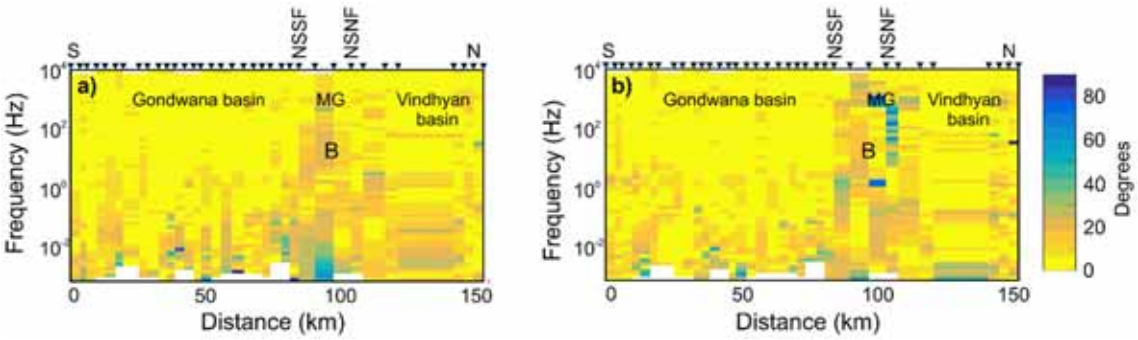

Figure 14. Pseudosection of sin θ (real and imaginary components) derived from the MT data from Rewa–Shahdol region. Color scale indicates the range of angle. The real component is plotted in the left (**a**) and the imaginary component is plotted to the right (**b**). High values of sin θ ('B' in this figure) are observed in the NSL region comprising of NSSF and NSNF. MG: Mahakoshal Group of rocks.

6.2 *Type-II plot*

As discussed in the synthetic study, plotting Mohr circle on common axes for all frequencies demonstrate the effects of noise in MT data. Based on the synthetic study results, to know the existence of noise in the present data set, we plot the Mohr circle on common axes (figure 12a–e (A)) for five (R1, R2, R3, R4, and R5) MT stations. In Type-II plot, all the five stations data possess a random behavior along with their respective coordinates; the behavior establishes the existence of noise in the data set (figure 12a–e (A)).

Further, plotting of Mohr circle properties with respect to the frequency is shown in figure 12(a–e (B)). The properties plot for the MT data shows fluctuations in real and imaginary parts; nevertheless, the fluctuations are exhibiting some trend. Except for R2 station, remaining stations' real and imaginary parts of plots show 1-D signature at high-frequency (both D and R-values lie close to zero). The existence of noise in the data does not allow the criteria of 1-D to be fulfilled, for instance, R4 and R5 exhibit fluctuations in D and R values (red color rectangular box in figure 12d (B)). The plots indicate 2-D signature in real components, i.e., radius values move off and D values being on the horizontal axis for the data in the frequency range 10–0.1 Hz. The three-dimensional signature appears at the lower frequency (beyond 0.1 Hz) of the real part as D and R values move away (non-zero) from the horizontal axis; the imaginary part of plots concur with real part results at this frequency range. Error-values for radius and center points of Mohr circle increase largely over lower frequency, these errors coincide with error bars in apparent resistivity and phase data at the lower frequency.

7. Pseudosection of tan ϕ and sin θ

A pseudosection of tan ϕ along the profile is shown in figure 13. Few anomalous features are observed from both (real and imaginary) pseudosections (figure 13a and b). Feature 'A' which is in the NSL zone, shows 2-D or 3-D signature throughout the frequency range may indicate the horst feature. This feature can be seen from the apparent resistivity pseudosection (figure 15). Further, at the lower frequency (>1 Hz), the whole data set shows a 2-D or 3-D signature of the basement structure. Deposition of Gondwana and Vindhyan sediments in the graben on either side of the NSL zone is reflected as a 1-D structure in the high-frequency range. In the real part of tan ϕ, the 1-D feature is observed in between two faults, which indicates the Mahakoshal group rocks. To differentiate the 2-D and 3-D signature in the study area, pseudosection of sin θ (real and imaginary) generated for the entire profile, as shown in figure 14(a and b). For the high-frequency range, the angle shows 1-D or 2-D signature in real and imaginary parts along entire profile except in the NSL zone where most of the stations show weak 3-D or strong 2-D structure at the high-frequency in both real and imaginary components. The invariants tan ϕ and sin θ together suggest a 1-D structure up to 10 Hz at all the stations except NSL zone, beyond that, 2-D/3-D signature appears including NSL zone that gives the evidence of the horst-graben structure of the study area with basement undulations. Tectonic activities such as subduction of Bastar craton below the Bundelkhand craton may have brought out undulation of basement structure below the Gondwana sediments, and flat nature of basement below the Vindhyan shows the absence of structural disturbance in Northern part of NSL.

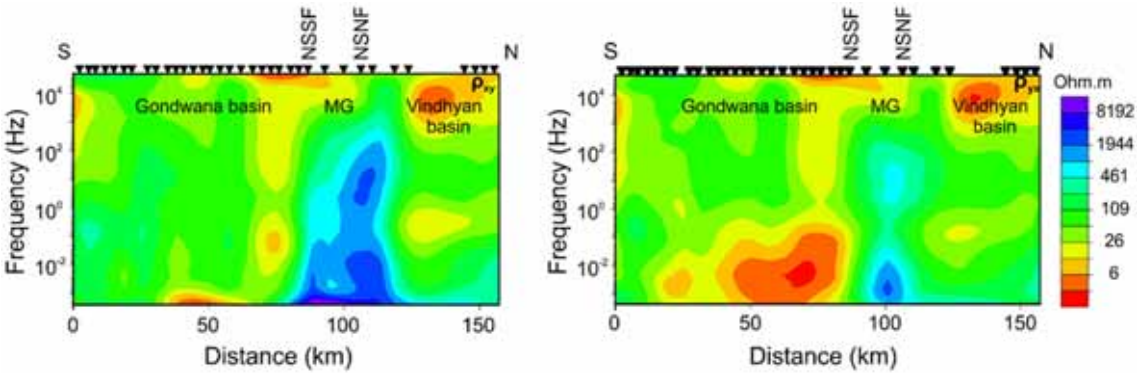

Figure 15. Pseudosections of apparent resistivity (ρxy and ρyx) along the profile in Rewa–Shahdol region.

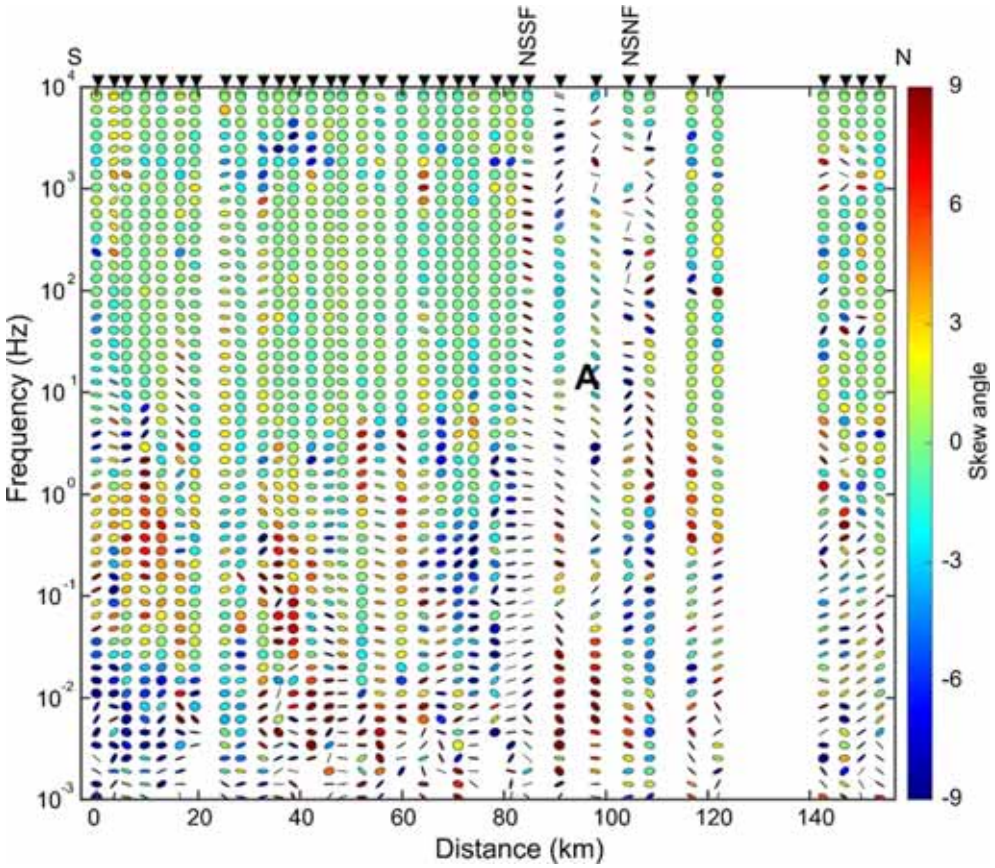

Figure 16. Skew filled phase tensor ellipses for all the MT sites along the profile in Rewa–Shahdol region. Anomalous skew values and the phase tensor ellipses are seen in the NSL zone ('A').

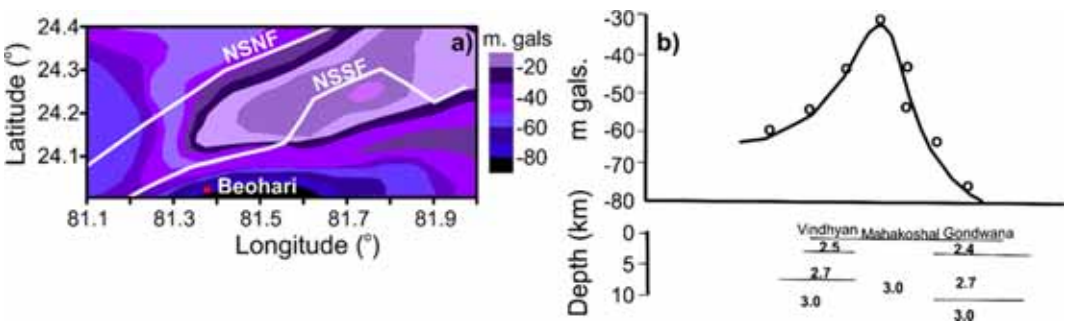

Figure 17. (**a**) Bouguer gravity contour map of NSL zone obtained from Qureshy and Warsi (1975) and (**b**) Gravity model across the profile (see the profile direction in figure 9) in the NSL zone (CRUMANSONATA 1995).

7.1 *Correlation with phase tensor*

Phase tensor represents 1-D and isotropic when the ellipse is a circle. In the 2-D case, the principal axes are not equal, and the skew angle will be zero ($\beta = 0$). In the general (3-D) case, the skew angle (β) is non-zero, and the phase tensor ellipse is non-symmetric. Phase tensor parameters were computed for Rewa–Shahdol region MT data to correlate the results of the Mohr circle. It may be seen from figure 16 that the region below the NSL shows 2-D/3-D signature ('A' in figure 16) for an entire frequency range. Rest of the area, we observed 1-D structure at a shallow level and 2-D/3-D signature at the deeper level. The phase tensor results show similar to Mohr circle results.

7.2 *Implications of dimensionality*

Very few geophysical studies (Qureshi and Warsi 1975; CRUMANSONATA 1995) were conducted in the present study area. Hence, we considered previous studies, i.e., seismic and MT (Kaila *et al.* 1987; Murty *et al.* 1998; Patro and Sarma 2016) in the western part of the present study area to validate the dimensionality characteristics of Rewa–Shahdol region. Results of basement upliftment in the form of horst (Kaila *et al.* 1987; Murty *et al.* 1998) and emplacement of different geometries of bodies below the NSL (Patro and Sarma 2016) show heterogeneity characteristics of crustal level which is represented by high dimensionality feature (figures 11–16) in the present study. Qureshi and Warsi (1975) proposed that two gravity low on either side of the gravity high between the NSSF and NSNF showing the horst structure with a Gondwana and Vindhyan graben either side of it (figure 17a). Later on, gravity studies carried out under project CRUMANSONATA (1995) across the NSL zone, and the gravity profile overlap with a part of the present MT profile as shown in figure 9. The study brought out a high gravity below the NSL and low gravity on either side of it representing rift zone with Mahakoshal group bounded by Vindhyan and Gondwana basins on either side (figure 17b). The Mohr circle analysis shows the sedimentary column of Gondwana and Vindhyan basins in the form of the 1-D structure on either side of high dimensionality nature of NSL. The collision of southern and northern cratons of peninsular India brought out the complex nature of crustal structure in the middle of the CITZ. The scenario of tectonic activity is represented by the undulation of high dimensionality nature of basement structure below the Gondwana basin (figure 13a and b). Whereas we do not observe such a crustal disturbance below the Vindhyan hence, we conclude that there was no major tectonic activity in the north of NSL.

8. Conclusions

Mohr circle is one of the tools among the graphical representation of impedance tensor. We examined Rewa–Shahdol region MT data to understand the dimensionality of the subsurface structure through the Mohr circle approach. Dealing of two types of Mohr circle plots such as a plotting of Mohr circle on the individual axes for each frequency (Type-I plot) represents the dimensionality of impedance tensor with respect to the frequency, and plotting of Mohr circle on common axes (Type-II plot) represents the influence of noise in the signal. In the synthetic analysis, Mohr circle Type-I plot fluctuates randomly and shows an irregular dimensionality information with respect to the frequency after adding the synthetic random noise to the good quality MT data. Type-II plot of the Mohr circle distinguish the noisy data and noise-free data in synthetic studies. In Type-I plot for Rewa–Shahdol region, MT data set shows a clear signature of NSL zone where all the stations exhibit 2-D structure for the high-frequency range and 3-D signature at low-frequency range in both real and imaginary components. Type-II plot shows the data quality where Mohr circle response moves randomly along x- and y-axes under the influence of noise. The proposed new invariants ($\tan\phi$, $\sin\theta$) can be represented by Mohr circle, and that assists in understanding the dimensionality of the subsurface structure as well as anisotropy and distortion in the MT dataset. The new invariants brought out subsurface dimensionality structure below the Rewa–Shahdol region in which the Narmada–Son lineament zone shows 2-D/3-D signature an entire frequency range. Except for NSL zone, rest of the area shows 1-D signature up to 10 Hz that is representing the Gondwana and Vindhyan sedimentary column. Large $\tan\phi$ values together with the phase tensor analysis, MT, seismic, and gravity studies, show the complexity of the NSL zone with high dimensionality, which has undergone successive rifting, and block movement.

Acknowledgements

We thank Director, CSIR–NGRI, for the constant encouragement and permission to publish this work. We are also thankful to K Chinna Reddy, Ujjal Kumar Borah and Sivamallaiah Sana for participating MT data acquisition. The study supported by a CSIR 12th five year plan project SHORE (PSC-0205), and MLP-6404-28 (BPK). KR's research is also supported through the CSIR–Senior Research Fellowship. We thank the anonymous reviewers and the associate editor for their suggestions, which improved the clarity in the paper.

References

Abdul Azeez K K, Unsworth M J, Patro P K, Harinarayana T and Sastry R S 2013 Resistivity structure of the Central Indian Tectonic Zone (CITZ) from multiple magnetotelluric (MT) profiles and tectonic implications; *Pure Appl. Geophys.* **170** 2231–2256.

Bayrak M, İlkışık O M, Kaya C and Başokur A T 2000 Magnetotelluric data in western Turkey: Dimensionality analysis using Mohr circles; *J. Geophys. Res., Solid Earth* **105(B10)** 23,391–23,401.

Borah U K, Patro P K and Suresh V 2015 Processing of noisy magnetotelluric time series from Koyna–Warna seismic region, India: A systematic approach; *Ann. Geophys.* **58(2)** G0222.

Chakraborty C, Mandal N and Ghosh S 2003 Kinematics of the Gondwana basins of peninsular India; *Tectonophys.* **377** 299–324.

Choubey V D 1971 Narmada–Son lineament, India; *Nature* **232(28)** 38–40.

CRUMANSONATA 1995 Project CRUMANSONATA: Geoscientific studies of the Son–Narmada–Tapti lineament zone; *Geol. Surv. India, Spec. Publ.* **10** 371p.

Gokarn S G, Rao C K, Gupta G, Singh B P and Yamashita M 2001 Deep crustal structure in central India using magnetotelluric studies; *Geophys. J. Int.* **144** 685–694.

Kaila K L, Murty P R K, Mall D M, Dixit M M and Sarkar D 1987 Deep seismic soundings along Hirapur–Mandla profile, central India; *Geophys. J. Roy. Astron. Sot.* **89** 399–404.

Lilley F E M 1976 Diagrams for magnetotelluric data; *Geophysics* **41** 766–770.

Lilley F E M 1993a Magnetotelluric analysis using Mohr circles; *Geophysics* **58** 1498–1506.

Lilley F E M 1993b Mohr circles in magnetotelluric interpretation (i) Simple static shift; (ii) Bahr's analysis; *J. Geomag. Geoelectr.* **45** 833–839.

Lilley F E M 1993c Three dimensionality of the BC87 magnetotelluric data set studied using Mohr circle; *J. Geomag. Geoelectr.* **45** 1107–1113.

Murty A S N, Mall D M, Murty P R K and Reddy P R 1998 Two-dimensional crustal velocity structure along Hirapur–Mandla profile from seismic refraction and wide-angle reflection data; *Pure Appl. Geophys.* **152** 247–266.

Naidu G D and Harinarayana T 2009 Deep electrical imaging of the Narmada–Tapti region, central India from magnetotelluric; *Tectonophys.* **476** 538–549.

Patro B P K, Harinarayana T, Sastry R S, Rao Madhusudan Manoj C, Naganjaneyulu K and Sarma S V S 2005 Electrical imaging of Narmada–Son Lineament zone, Central India from magnetotelluric; *Phys. Earth Planet. Inter.* **148** 215–232.

Patro P K and Sarma S V S 2016 Evidence for an extensive intrusive component of the Deccan Large Igneous Province in the Narmada–Son Lineament region, India from three-dimensional magnetotelluric studies; *Earth Planet. Sci. Lett.* **451** 168–176.

Qureshy M N and Warsi W E K 1975 Role of regional gravity surveys in a concept-oriented exploration programme: Some inferences from a study in a shield area of central India; *J. Geol. Soc. India* **16** 44–54.

Rao K V, Rama B V and Ramasastry P 1990 A geophysical appraisal of Mahakoshal group of upper Narmada valley; *Geol. Surv. India, Spec. Publ.* **28** 99–117.

Rao C K, Gokarn S G and Singh B P 1995 Upper crustal structure in the Torni–Purnad region, Central India, using magnetotelluric studies; *J. Geomag. Geoelectr.* **47** 411–420.

Rao C K, Ogawa Y, Gokarn S G and Gupta G 2004 Electromagnetic imaging of magma across the Narmada–Son lineament, central India; *Earth Planets Space* **56** 229–238.

Roy A and Bandyopadhyay B K 1990 Tectonic and structural pattern of the Mahakoshal belt of central India: A discussion; *Geol. Surv. India, Spec. Publ.* **28** 226–240.

Roy A and Prasad M H 2001 Precambrian of Central India: A possible tectonic model; *Geol. Surv. India, Spec. Publ.* **64** 177–197.

Roy A and Prasad M H 2003 Tectonothermal events in Central Indian Tectonic Zone (CITZ) and its implications in Rodinian crustal assembly; *J. Asian Earth Sci.* **22** 115–129.

Simpson F and Bahr K 2005 Practical magnetotellurics, Cambridge University Press, 82p.

West W D 1962 The line of Narmada–Son valley; *Curr. Sci.* **31** 143–144.

Corresponding editor: Arkoprovo Biswas